Macromolecules

Article

pubs.acs.org/Macromolecules

Polymer/Pristine Graphene Based Composites: From Emulsions to Strong, Electrically Conducting Foams

Steven J. Woltornist,[†] Jan-Michael Y. Carrillo,[§] Thomas O. Xu,[†] Andrey V. Dobrynin,*[,‡] and Douglas H. Adamson*[,†,‡]

[†]Department of Chemistry and [‡]Polymer Program, Institute of Materials Science, University of Connecticut, Storrs, Connecticut 06269, United States

[§]National Center for Computational Science, Oak Ridge National Laboratory, Oak Ridge, Tennessee 37831, United States

Supporting Information

ABSTRACT: The unique electrical, thermal, and mechanical properties of graphene make it a perfect candidate for applications in graphene/graphite based polymer composites, yet challenges due to the lack of solubility of pristine graphene/graphite in water and common organic solvents have limited its practical utilization. Here we report a scalable and environmentally friendly technique to form water-in-oil type emulsions stabilized by overlapping pristine graphene sheets, enabling the synthesis of open cell foams containing a continuous graphitic network. Our approach utilizes the insolubility of graphene/graphite in both water and organic solvents and so does not require oxidation, reduction, surfactants, high boiling solvents, chemical functionalization, or the input of large amounts of mechanical energy or heat. At the heart of our technique is the strong attraction of graphene to high-energy oil and water interfaces. This allows for the creation of stable water-in-oil emulsions with controlled droplet size and overlapping graphene sheets playing the role of surfactant by covering the droplet surface and stabilizing the interfaces with a thin graphitic skin. These emulsions are used as templates for the synthesis of open cell foams with densities below 0.35 g/cm^3 that exhibit remarkable mechanical and electrical properties including compressive moduli up to ∼100 MPa, compressive strengths of over 8.3 MPa (1200 psi), and bulk conductivities approaching 7 S/m.

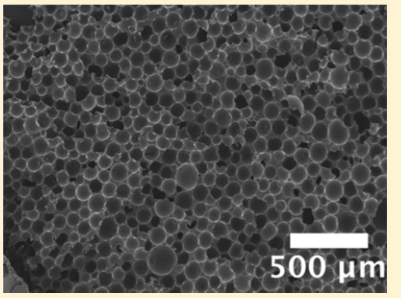

INTRODUCTION

The excitement surrounding the potential of graphene as a nanofiller in composite materials is driven by its unique set of electrical and mechanical properties.[1−9] A common theme in previous studies of graphite and graphene based composites has been that the lack of graphene solubility is viewed as a challenge to be overcome. Solutions to graphene's insolubility include employing graphene oxide (GO) or reduced graphene oxide (rGO),[10−16] harsh *in situ* chemical reduction steps,[17,18] the use of high boiling and difficult to remove solvents,[19] and extended sonication treatments that result in the breaking of sheets from shear stress.[20] All of these approaches pay a price in terms of degraded graphene properties. An approach that does not view graphene's insolubility as a limitation and thus utilizes pristine, unaltered graphite would have major advantages in terms of properties, cost, and environmental impact.

In this article, we report the results of a combination of experimental, theoretical, and computational techniques to demonstrate the affinity of pristine graphene sheets to a water−oil interface and describe the use of this surface activity to stabilize water-in-oil emulsions. In particular, we take advantage of graphene/graphite's inherent insolubility and the large interfacial energies between aqueous and organic solvents by adding graphite to a mixture of two immiscible solvents and observing the spreading of graphene sheets at the high-energy liquid−liquid interface, where the spreading is driven by a lowering of the total free energy of the system. The sheets then become trapped at the interface of the two solvents, playing the role of a stabilizing agent for emulsions of water droplets dispersed in a continuous oil phase. In this context graphene sheets can be viewed as two-dimensional surfactants with internal bending rigidity.

Although, to the best of our knowledge, the stabilization of emulsions by pristine graphene sheets has not been demonstrated previously, there are recent reports of GO being used as an emulsion stabilizer. The emulsions created with GO or GO derivatives are oil-in-water emulsions, as opposed to the water-in-oil emulsions we find with pristine graphene. This results in the formation of spherical polymer beads coated with GO being produced rather than a continuous composite material when the oil phase is polymerized in the GO based emulsions. For instance, Gudarzi et al. produced a "nanocomposite powder" with GO and PMMA,[21] Dao et al. synthesized surface functionalized rGO to make "microspheres",[22] Zhang et al. used functionalized rGO to make a PS based "solid powder",[23] and Yin et al. reported GO coated PS microspheres.[24] A recent extensive study of GO stabilized emulsions concluded that GO emulsions were best described as Pickering emulsions and that only oil-in-water emulsions were formed.[25]

Received: December 1, 2014

DOI: 10.1021/ma5024236
Macromolecules XXXX, XXX, XXX−XXX

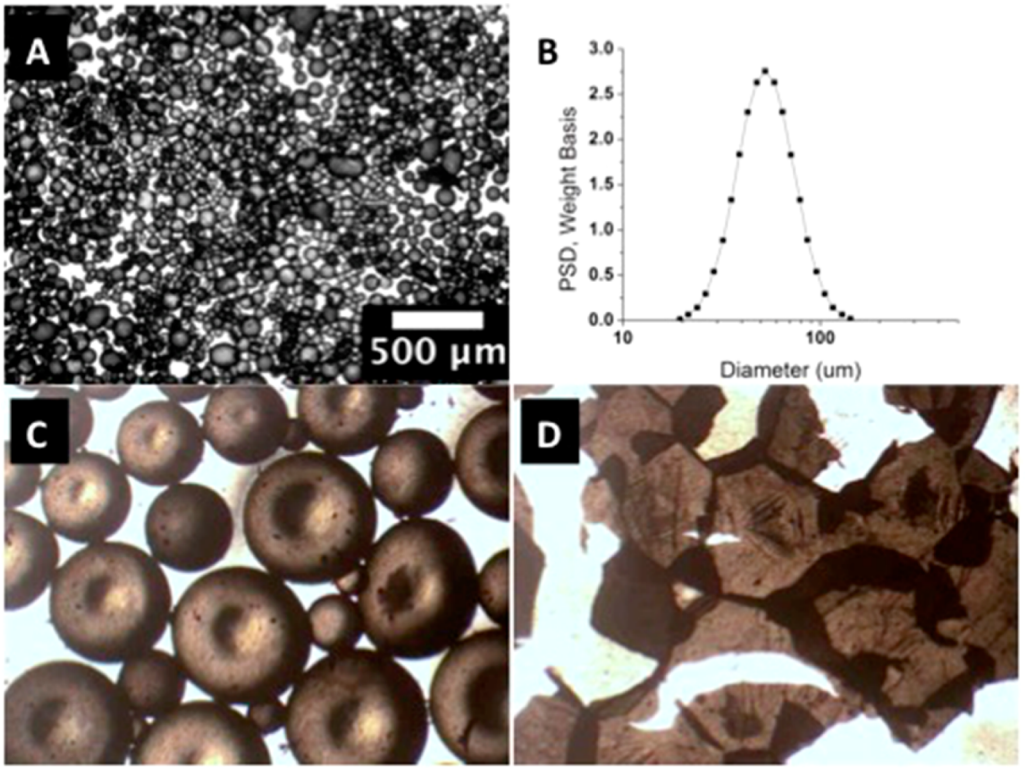

Figure 1. Graphitic skin stabilized emulsions. (A) Optical microscopy image of graphitic skin stabilized emulsion in 50:34:0.44 mass ratio water/heptane/graphene mixture. (B) Droplet size distribution of graphite skin covered water droplets with average diameter 55 μm in 50:34:0.44 mass ratio water/heptane/graphene mixture as determined by acoustic measurements. (C) Magnified optical microscopy image of the initial structure of the water droplets covered with graphene skin before heptane evaporation. (D) Optical image of the graphitic skin left behind after heptane evaporation and droplet burst.

Using a monomer as the oil phase, we demonstrate how pristine graphene stabilized water-in-oil emulsions template solid graphite composite foams. After polymerization of the continuous phase, the water-filled spherical cavities are lined with a graphitic skin consisting of overlapping pristine graphene sheets. A gentle evaporation process removes the water, leaving a final open cell foam composite with exceptional mechanical strength, electrical conductivity, and low density, with cells sizes easily controllable by varying the mixture composition. This environmentally friendly approach to graphite utilization in polymer composites avoids the use of chemical treatments, the input of large amounts of mechanical or thermal energy, or the addition of stabilizers such as surfactants or high boiling solvents that can be difficult to remove. Potential applications of these low-cost materials include strong and lightweight building materials, filters, ultracapacitor electrodes, and conductive catalyst supports.

RESULTS AND DISCUSSION

The affinity of graphene sheets to a water/oil interface and their emulsion stabilization is studied with emulsions formed by water/heptane/graphite mixtures. Emulsions are produced as described in the Methods section. Figure 1A shows the structure of a graphite stabilized water-in-heptane emulsion under optical microscopy. Heptane is the continuous phase surrounding graphitic skin stabilized spherical water droplets with diameters varying between 20 and 200 μm. Note that there is some coalescence during the transfer process to the glass slide needed for imaging. The droplet size distribution in a water-in-heptane emulsion can be seen in Figure 1B.[26] The average size of the droplets is 55 μm, which is consistent with optical image analysis of the resultant emulsion shown in Figure 1A. That the water droplets are stabilized with a graphitic skin and not by chunks of graphite is shown in Figures 1C,D. These images of droplets before and after bursting upon evaporation of the heptane continuous phase clearly show the skin surrounding the droplets is made of sheets, not by graphite particles. Further, the skin displays different degrees of transparency, indicating differences in the number of sheets forming the skin and providing strong evidence for skin thicknesses of a few graphene layers.

Corroborating the observation of few layer thick skin are results of our recent all atom molecular dynamics simulations of graphene flakes in a water/heptane mixture.[27] These simulations show that graphene flakes associate at the water/heptane interface forming stacks consisting of two to three graphene flakes. These graphene stacks are localized at the water/heptane interface with slight preference toward the heptane phase. The system free energy change required to move a graphene flake into the heptane phase is $|\Delta g| \approx 2.2$ mN/m. Thus, for a 100×100 nm graphene sheet, the work required to move it from the water/heptane interface into the heptane phase is on the order of 5300 $k_B T$ (where k_B is the Boltzmann constant and $T = 300$ K). Note that the penalty to move a graphene sheet into a water phase would be even higher. This energy cost effectively traps the graphene sheets at the water/heptane interface, a phenomenon similar in some ways to the trapping of nano- and microparticles at a water/oil interface in Pickering emulsions.[28]

In order to compare graphene affinity in heptane/water emulsions with that in the styrene/water emulsions used to make the reported composites, we have performed all atom molecular

DOI: 10.1021/ma5024236
Macromolecules XXXX, XXX, XXX−XXX

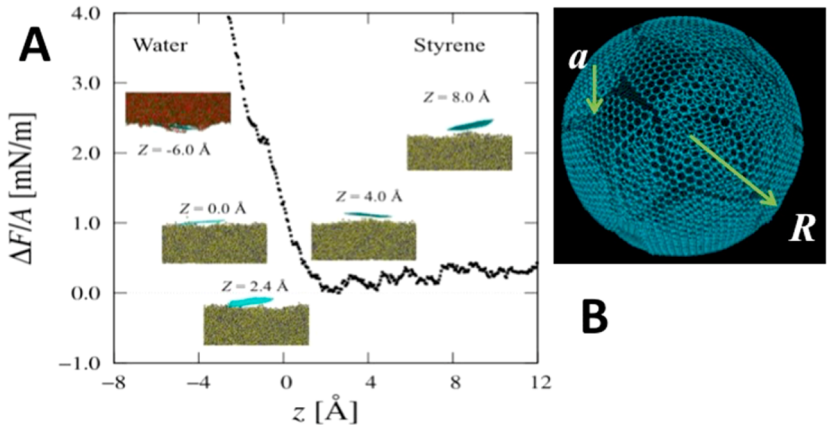

Figure 2. (A) Potential of the mean force for a graphene flake calculated along z-axis normal to water/styrene interface. Insets show typical graphene flake configurations. The solvent into which the graphene flake is pulled is transparent. In the insets, the hydrogen atoms of water molecules are yellow, oxygen atoms of water are blue, the carbon atoms belonging to styrene are red, and the hydrogen atoms of styrene are green. Graphene flakes are shown in cyan. (B) Schematic representation of a water droplet with size R covered with a graphene skin formed by flakes of size a.

dynamics simulations to calculate the potential of the mean force between a graphene flake and water/styrene interface. In these simulations we use the generalized Amber force field[29] for the atomistic model of styrene and graphene. The graphene flake is modeled as a polycyclic aromatic hydrocarbon consisting of eight generations of carbon rings terminated by hydrogen, $C_{384}H_{48}$.[27,30] The partial charges on the styrene and the graphene flakes are obtained from the Mulliken population analysis from *ab initio* calculations using the Gaussian09 simulation package with the 6-31G(d) basis set and B3LYP DFT method[31] as described in the work of Woltornist et al.,[27] Oyer et al.,[30] and section SI1 of the Supporting Information. For water we use the TIP3P force field potential.[32] The system consists of 9360 water molecules, 1360 styrene molecules, and one graphene sheet. The simulations are performed following methodology developed for modeling of the graphene flakes in heptane/water mixture,[27] with details of the simulation procedure described in section SI1. In order to determine the surface activity of a graphene sheet in a water/styrene system, the weighted histogram analysis method[33] is used to calculate the potential between the graphene sheet and the water/styrene interface.

All simulations are performed at constant temperature T equal to 300 K. The variation of the potential of the mean force along the z-axis normal to the interface is shown in Figure 2A. The minimum of the potential is located in the styrene phase, indicating that although insoluble in both phases, the preference of graphene is for styrene rather than water. The increase of the potential in the styrene phase is not as steep as that observed in the water phase, another indication that styrene is a better solvent for graphene than is water. Oscillations seen in the potential of mean force indicate displacement of the aligned styrene molecules as the graphene flake is moved further away from the interface. The magnitude of the potential in the plateau regime is on the order of $|\Delta g| \approx 0.4$ mN/m. It is important to point out that similar calculations done for the heptane/water mixtures show that this free energy change is even higher $|\Delta g| \approx 2.2$ mN/m for that system.[27] Using these values, we can estimate the work required to displace a 100 × 100 nm graphene sheet from the water/styrene interface into the styrene phase to be 966 k_BT, sufficiently strong to trap graphene sheets at the water/styrene interface. The work required to displace the graphene sheet into a heptane phase is about 6 times larger.

To model the total potential of the mean force in our system, we consider an emulsion prepared by mixing oil, water, and graphite with masses m_0, m_w, and m_g, respectively. The emulsion composition can be characterized by two mass ratios of graphene to water, $\phi_g = m_g/m_w$, and water to oil, $\phi_{w/o} = m_w/m_0$. The oil forms a continuous phase surrounding the water droplets with size R. Each water droplet is covered by a graphitic skin of thickness h which is made of graphene sheets with average size a (see Figure 2B). The thickness of the graphitic skin h depends on the size R of the water droplets due to the mass conservation requirement such that $h = \beta R/3$, where we introduced parameter $\beta = \phi_g\rho_w/\rho_g$ with $\rho_w = 1.0$ g/cm^3 and $\rho_g = 2.66$ g/cm^3 being mass densities of water and graphene respectively (see section SI2 for details). The volume of emulsion per water droplet V_0 can be expressed in terms of the emulsion composition $\phi_{w/o}$, where $V_0 = 4\pi\alpha R^3/3$ with parameter $\alpha = 1 + \rho_w/\phi_{w/o}/\rho_o$ and ρ_o is the oil mass density. Thus, in the emulsion occupying volume V there are V/V_0 water droplets with size R. The total free energy change due emulsion formation is the sum of contributions from individual droplets (see section SI2 for derivation details). It has contributions from the graphitic skin bending energy and from the change of the oil/water interface free energy due to bringing graphene sheets to the interface. Equation 1 describes the result:

$$\frac{\Delta F_{total}}{V} \approx \frac{E}{384}\frac{\beta}{\alpha}\frac{a^4}{R^4} - \frac{3|\Delta g|}{\alpha R} \quad (1)$$

where E is the Young's modulus of the graphene sheet (~1 TPa). It follows that the affinity of the graphene toward the water/oil interface promotes the formation of smaller droplets to maximize the system free energy gains. However, graphene sheets adsorbed at the surface of smaller droplets have to bend more in order to remain at the interface, producing a bending energy penalty for each graphene sheet covering the surface of a droplet.

The size of the emulsion droplets is thus determined by a balance between the affinity of the graphene toward the solvent interface and the rigidity of the graphene sheets. The optimal size of the droplets is obtained by optimizing the system free energy ΔF_{total} with respect to droplet size R:

$$R^* \approx \left(\frac{E\beta a^4}{288|\Delta g|}\right)^{1/3} \quad (2)$$

DOI: 10.1021/ma5024236
Macromolecules XXXX, XXX, XXX−XXX

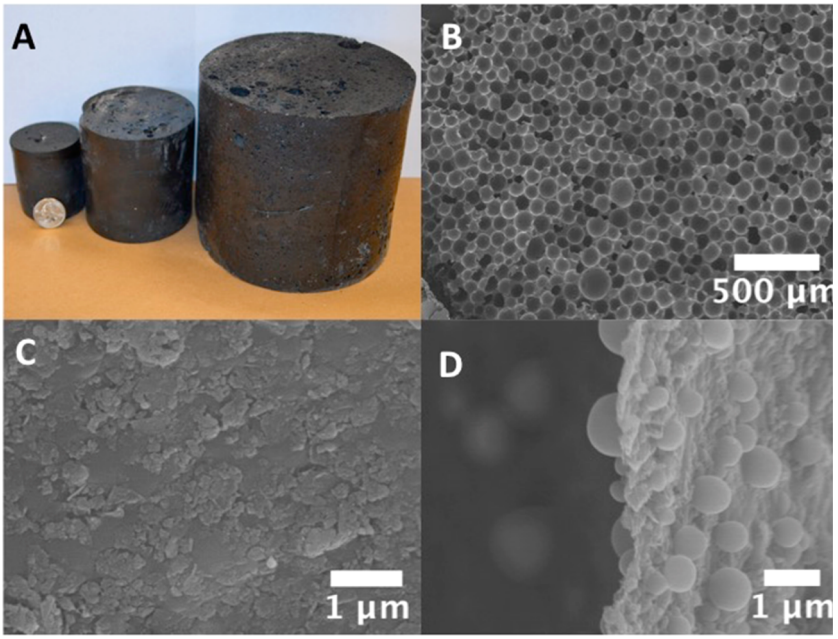

Figure 3. Composite foam morphology. (A) Graphene composite foams of various sizes with a US quarter for scale. (B) Scanning electron micrograph of a cross section of the composite after polymerization made from an emulsion with a 50:34:0.44 mass ratio of water/styrene/graphite. (C) Graphene sheets seen lining the inside of the spherical cavities of the composite foams. (D) Micrograph of a cross section of a sphere−sphere contact point. The small spheres seen on both sides of the graphitic skin arise from the very small amount of styrene solubilized in the water phase.

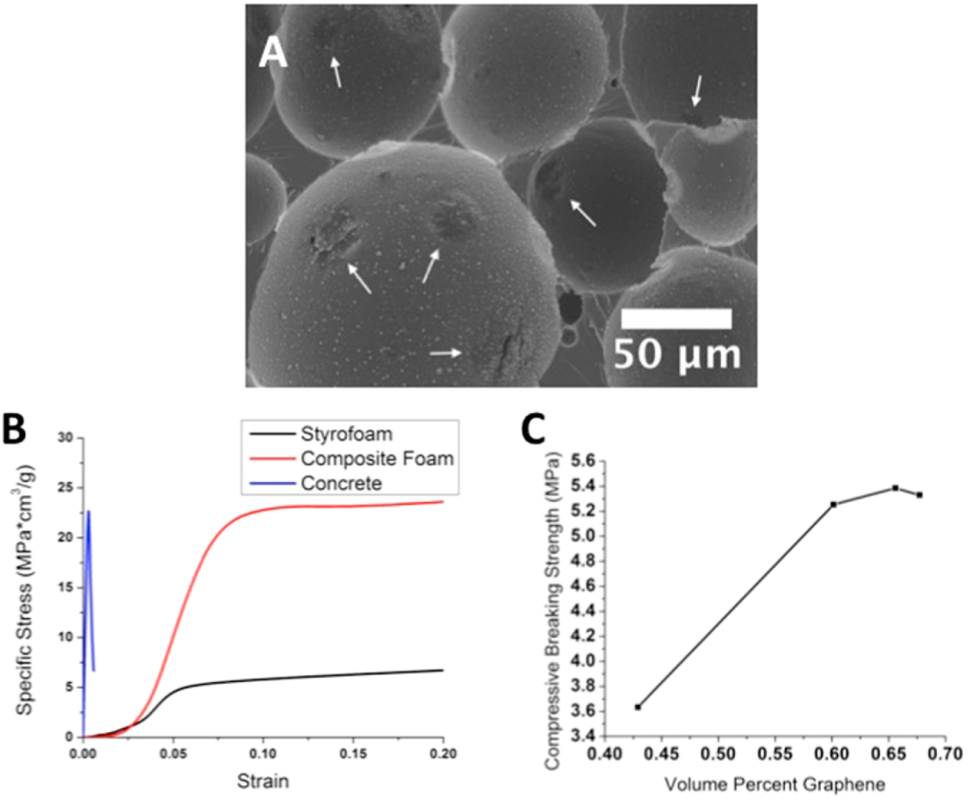

Figure 4. Morphology and compressive strength. (A) Scanning electron micrograph of a composite foam with visible sphere−sphere contact points indicated with arrows. These areas often sag because of the lack of supporting polymer. (B) Stress/strain curves of the composite foam and other industrial materials normalized by material density.[38] (C) Compressive strength vs volume percent graphite of the composite samples.

Equation 2 shows that we can control the size of the droplets by changing the graphene/water ratio (changing parameter β), by varying the graphene sheet size a, or by changing the identity of the oil. For example, in an emulsion with about 1% weight fraction of graphite with respect to water, $\beta \approx 0.0033$, of radius $a = 1.4\ \mu$m, we can estimate the diameter of the droplets in a water/heptane mixture to be on the order of 54 μm. This estimate is consistent with the emulsion droplet size of 55 μm observed

DOI: 10.1021/ma5024236
Macromolecules XXXX, XXX, XXX−XXX

Table 1. Water/Styrene Ratio Study

ratio water/styrene (volume)	ratio water/graphite (mass)	observed sphere diameter (μm)	density (g/cm^3)	compressive strength (MPa)	conductivity (S/m)	loading percent (by TGA)
1/1	114	90	0.26	5.33	0.043	5.73
3/2	136	130	0.27	5.25	0.051	4.90
7/3	159	160	0.30	5.38	0.054	4.81
3/1	170	190	0.22	3.63	0.070	4.29
4/1	182		0.15	1.07	0.148	8.76

experimentally (see Figure 1B). Repeating the same calculations for a water/styrene mixture, we estimate the diameter of the droplets to be 95 μm. This is consistent with the image shown in Figure 3B of a foam resulting from an emulsion with 80−90 μm diameter droplet sizes. Note that the increase in the droplet size is consistent with a decrease in the graphene flake affinity to the water/oil interface in these two systems. However, this is only an estimate for the size of the droplets covered with the graphitic skin. In reality, the droplets in the emulsions could be smaller due to droplets' breakup upon emulsion shearing in homogenizer.[34] Indeed, we see a decrease followed by saturation of the average droplet size with increasing homogenization time.

The same approach is used to make emulsions with styrene as is used to make emulsions with heptane. In both cases, the graphitic skin stabilized water droplets settle to form a densely packed phase of spheres with the oil phase filling the space between them. The aggregation between graphitic skin covered droplets is due to van der Waals attraction between graphene sheets forming the skin layer. The excess of the oil phase forms a pure liquid phase above the emulsion, and the densely packed emulsion phase remains stable as confirmed by measuring G' at extended time (see section SI3 for details).

In the case of styrene as the oil phase, gentle heating polymerizes the oil phase. After the styrene monomers are polymerized, the graphitic skin covered water droplets are fixed in space, forming a rigid foam. This approach is highly scalable as illustrated in Figure 3A showing composites of increasing overall size, all with the same underlying foam structure. A cross-sectional image of a typical graphene foam using a JEOL 6330 field emission scanning electron microscope (FESEM) is shown in Figure 3B. The imaged surface is much like the surface of a golf ball, with concave divots covering the entire surface. A higher magnification image of the interior of a divot, shown in Figure 3C, clearly shows a layer of graphene sheets lining the interior of the cavities. Figure 3D shows where the emulsion droplets make contact, with little or no polymer observed, only a thin layer of overlapping graphene sheets. This structural feature is crucial to the electrical conductivity of the composites as it provides the contact between graphene sheets of different spheres. The spheres observed on the surface of the graphitic skin in Figure 3D are the result of a very small amount of dissolved styrene in the water phase that polymerizes and precipitates out. This is verified by the addition of NaCl to the water phase, reducing the solubility of styrene and resulting in nearly no small polystyrene spheres being observed in the composite (see section SI4).

The placement of these thin contact regions can be seen in Figure 4A. In some instances a tear can be observed in the graphitic skin, providing a pathway for water removal. If gentle heat is applied, these regions provide ample space for water to escape. Placing the water wet material in high vacuum, however, causes the water to burst out of the spheres, creating a popcorn-like effect. These openings between spheres also allow for the infusion of various polymers into a dried foam. Adding a second polymer to the inside surface of the spheres, along with controlling the average size of the spheres, provides a powerful handle for tuning the mechanical and electrical properties of the foams. A comparison of the specific stress of the foams versus those of concrete and Styrofoam may be seen in Figure 4B. The foams are seen to have both the specific strength of concrete and the plateauing failure mechanism of Styrofoam. As the graphene content increases, the compressive breaking strength increases until it reaches a local maximum, as seen in Figure 4C.

The sphere size is controlled by altering the ratio of styrene to water in the emulsion as well as by varying the amount of graphite. Table 1 shows the progression of sphere sizes from a 4/1 to a 1/1 water/styrene ratio with a constant graphene concentration. The graphene concentration dependence of sphere size is shown in section SI5. The relative amount of each solvent in the initial mixture also determines the volume fraction of the emulsion phase in the total mixture. For a 7/3 water/styrene ratio, the final volume of the sample is composed almost entirely of the emulsion. If the volume fraction of the water is less than 7/3, the system has an excess styrene phase and spheres become smaller. When the volume fraction of water is raised above 3/1, the emulsion loses its stability and the graphene spheres coalesce, leaving an excess of water and a larger average sphere size. At a 9/1 ratio and above, the emulsion structure is lost. The relationship between solvent volume ratio and emulsion volume fraction is plotted in section SI6.

The sphere size of the foams is strongly correlated with both compression strength and electrical conductivity, with foams composed of spheres smaller than ~160 μm diameter having a higher compressive strength than foams with larger spheres. At diameters greater than ~190 μm, the emulsions begin to coalesce and the volume fraction of the emulsion in the mixtures becomes smaller. At a 4/1 ratio, the regular foam structure is nearly gone and an average sphere size cannot be determined. Even though the composite contains a large fraction of graphite, the collapse of the regular sphere structure results in a weak material. Our material compares favorably to commercial materials formed by dispersing graphite flakes in foamed polystyrene have compressive resistances on the order of 0.173 MPa at 10% yield.[35]

Unlike the mechanical strength, the electrical conductivity is observed to depend on the overall level of graphene loading rather than on the spherical structure of the foam. This results in larger sphere foams showing increased conductivity as the emulsion phase gets smaller while the amount of graphene stays constant. The densely packed sphere structure of the graphene foam composite allows for electrical conductivity at low graphene loadings, although increased graphite loading levels in non-optimal systems can also lead to highly conductive material.

Increasing the conductivity and mechanical properties of the foams is also achieved by the addition of a second polymer to the interior of a previously dried foam. The passageways for the removal of water provide an opportunity to infuse a second

DOI: 10.1021/ma5024236
Macromolecules XXXX, XXX, XXX−XXX

polymer into the system. Submerging a composite sample in a polymer solution and placing the system under gentle vacuum, the solution replaces the air in the foam. Subsequent removal of the solvent leaves behind the dissolved polymer from the solution. Infusing the graphene composite foam with an aqueous suspension of poly(3,4-ethylenedioxythiophene):poly-(styrenesulfonate) (PEDOT:PSS), followed by evaporation of the water, leaves a layer of PEDOT:PSS lining the interior surfaces of the foam. After the water evaporates, the PEDOT:PSS left behind is "draped" over the PS beads and graphene sheets as shown in section SI7. A dramatic increase in conductivity and compressive strength is observed, with conductivities improved by up to 2 orders of magnitude, from 0.07 to 7 S/m for a 3/1 initial water volume fraction sample. Compressive strengths are also improved by as much as 20%.

Although the graphene foam composite described uses water with styrene as the oil phase, many other monomers have been used. These include isoprene, butyl acrylate, divinylbenzene, and butyl methacrylate. Flexible foam composites are observed with polyisoprene, and ultralow densities are realized with butyl acrylate.

■ CONCLUSION

We have demonstrated the ability of graphene to serve as a surfactant for the stabilization of water-in-oil emulsions and used this ability to form low density, conductive, high compressive strength graphene/graphite polymer composites. A conductive network with low graphite loading is formed by the contact between thin graphitic skins surrounding the droplets of the close-packed dispersed phase. Computational results indicate an interface trapping mechanism operates to form the emulsions that serve as the composite template. Additionally, we demonstrated that the electrical conductivity and strength of the composite foams may be increased dramatically through control of the emulsion droplet size and the infusion of additional polymers such as PEDOT. The foams are inexpensive, and their formation is environmentally friendly with no volatile organic solvents, oxidations, reductions, high temperatures, or large input of energy required.

Limitations on the choice of monomer comes from the requirement that graphene stabilize the oil/water interface.[27] The oil phase must have a surface energy less than the surface energy of graphene and be nearly insoluble in the water phase. As graphene has a surface energy of 54.8 mN/m,[36,37] and water has a surface energy of 72.9 mN/m, the surface energy of the oil phase must be below 54.8 mN/m. The low surface energy of styrene and most other monomers easily fit this criterion, making the described approach both robust and diverse. Applications such as strong and lightweight building materials, ultracapacitor electrodes, conductive catalyst supports, and filtration are expected to be enabled by these materials and are currently being investigated.

■ METHODS

Sample Preparation. *Polystyrene/Graphene Composites.* For a typical graphene composite foam, a flask was charged with 880 mg of graphite (Asbury Carbons grade 2299, although others such as Asbury Carbons Micro 890 and 3243 have been used successfully as well), along with 150 mL of water (Deionized), 50 mL of styrene (Acros Organics, 99.5%), 12 mL of divinylbenzene (Aldrich, 80%), and a stir bar. The contents were then mixed on a stir plate for 30 s, followed by 30 s of bath sonication (Branson 80W B2510DTH). This procedure results in a graphene concentration of 4.4 mg/mL and a 3/1 water/styrene ratio. Composites with other ratios and concentrations are simply adjusted accordingly. The sonication was not necessary to obtain emulsions but utilized simply to break up large clumps of graphite. 150 mg of azobis(isobutyronitrile) (AIBN) (Aldrich, 98%) was then added to the same flask. The system was then mixed on a stir plate for a minimum of 15 min while being purged with Ar gas (Fisher). After the purging process, the contents of the flask were poured into a Waring commercial blender (Model 33BL79) under an Ar atmosphere. The blender was then turned on for 1 min. The newly formed emulsion was placed into a 250 mL jar and sealed under Ar gas. The jar was then placed in an oven (Thermo Electron Corporation, Model 6500) at ~70 °C for 24 h. After the reaction was complete, the composite samples were removed from the jars and heated at ~80 °C for ~2 days to remove all water. Excess bulk polystyrene was cut off of the top if necessary.

Characterization. *Emulsion Droplet Size Analysis.* The size of the dispersed aqueous phase droplets was determined with a DT-100 acoustic spectrometer from Dispersion Technology Inc. The attenuation spectra were analyzed using Dispersion Technology software for polydisperse emulsions.[26] The distribution was obtained from ultrasound attenuation spectra in the frequency range between 1 and 100 MHz.

The emulsion sample used in the measurement utilized heptane rather than styrene as the continuous phase. A flask was charged with 880 mg of graphite (Asbury Carbons grade 2299), along with 150 mL of water (Deionized), 62 mL of heptane (Fisher Optima), and a stir bar. The contents were then mixed on a stir plate for 30 s, followed by 30 s of bath sonication (Branson 80W B2510DTH). The sonication was not necessary to obtain emulsions but utilized simply to break up large clumps of graphite. The system was then mixed on a stir plate for about 30 s. After the mixing, the contents of the flask were poured into a Waring commercial blender (Model 33BL79). The blender was then turned on for 1 min. The contents were then poured into a jar for transportation and then directly into the instrument.

Microscopic Characterization. To prepare composite samples for the electron microscope, they were first cut with a razor blade. The slices were then mounted on aluminum stubs and coated with Au/Pd in a sputter coater (Polaron Unit E5100). The samples were characterized with a JEOL 6330 field emission scanning electron microscope with a 10 kV accelerating voltage.

The emulsion samples in Figure 1A,C,D utilized heptane rather than styrene as the continuous phase as described above. A wide-mouth pipet was used to transfer some of the emulsion to a glass slide. These were then analyzed using a Nikon Labophot with an IDS UI-3370CP Color camera in full color (C, D) or monochrome (A) mode.

Electrical Measurements. To prepare the samples for electrical conductivity testing, they were first cut into rectangular prisms on the scale of a few centimeters in length. The ends were then covered with silver paint (Ted Pella) and allowed to dry. Copper tape (Ted Pella) was then attached to the silver contacts, and the resistance was measured using a Keithly Model 2420 sourcemeter.

Thermal Analysis. 20 mg of each of the composites was crushed to a fine powder and analyzed in a TA Instruments TGA Q-500 to determine the graphene loading. The sample was heated in a platinum pan in a nitrogen-filled chamber from 20 to 800 °C at 10 °C/min. The mass of the sample left at 700 °C was taken to be purely graphene, since all of the polymer burned off by this point.

Mechanical Measurements. To prepare the samples for testing, they were first cut into cylinders around 5 cm in diameter (the diameter of the glass jars they are prepared in) and a few centimeters in height. They were then tested using an Instron Model 5869 in compression mode.

■ ASSOCIATED CONTENT

Supporting Information

Stabilization of emulsions by graphene sheets, simulation details, Raman spectroscopy, graphene concentration studies, salt studies, droplet size distribution, initial solvent volume vs final phase volume. This material is available free of charge via the Internet at http://pubs.acs.org.

DOI: 10.1021/ma5024236
Macromolecules XXXX, XXX, XXX−XXX

AUTHOR INFORMATION

Corresponding Authors

*E-mail avd@ims.uconn.edu (A.V.D.).

*E-mail adamson@uconn.edu (D.H.A.).

Notes

The authors declare no competing financial interest.

ACKNOWLEDGMENTS

The authors are grateful to the National Science Foundation for financial support under grants DMR-1004576 and DMR-1111021. J.-M Y.C's contribution was sponsored by the Office of Advanced Scientific Computing Research, U.S. Department of Energy, and performed at the Oak Ridge National Laboratory, which is managed by UT-Battelle, LLC, under Contract No. De-AC05-00OR22725.

REFERENCES

(1) Geim, A.; Novoselov, K. *Nat. Mater.* **2007**, *6*, 183−192.

(2) Novoselov, K. S.; Geim, A. K.; Morozov, S. V.; Jiang, D.; Zhang, Y.; Dubonos, S. V.; Grigorieva, I. V.; Firsov, A. A. *Science* **2004**, *306*, 666−669.

(3) Novoselov, K. S.; Geim, A. K.; Morozov, S. V.; Jiang, D.; Katsnelson, M. I.; Grigorieva, I. V.; Dubonos, S. V.; Firsov, A. A. *Nature* **2005**, *438*, 197−200.

(4) Zhang, Y.; Tan, Y.-W.; Stormer, H. L.; Kim, P. *Nature* **2005**, *438*, 201−204.

(5) Balandin, A. a; Ghosh, S.; Bao, W.; Calizo, I.; Teweldebrhan, D.; Miao, F.; Lau, C. N. *Nano Lett.* **2008**, *8*, 902−907.

(6) Chatterjee, S.; Wang, J. W.; Kuo, W. S.; Tai, N. H.; Salzmann, C.; Li, W. L.; Hollertz, R.; Nüesch, F. A.; Chu, B. T. T. *Chem. Phys. Lett.* **2012**, *531*, 6−10.

(7) Lee, C.; Wei, X.; Kysar, J. W.; Hone, J. *Science* **2008**, *321*, 385−388.

(8) Lee, J.-U.; Yoon, D.; Cheong, H. *Nano Lett.* **2012**, *12*, 4444−4448.

(9) Stoller, M. D.; Park, S.; Zhu, Y.; An, J.; Ruoff, R. S. *Nano Lett.* **2008**, *8*, 3498−3502.

(10) Suk, J. W.; Piner, R. D.; An, J.; Ruoff, R. S. *ACS Nano* **2010**, *4*, 6557−6564.

(11) Boukhvalov, D. W.; Katsnelson, M. I. *J. Am. Chem. Soc.* **2008**, *130*, 10697−10701.

(12) Becerril, H. a; Mao, J.; Liu, Z.; Stoltenberg, R. M.; Bao, Z.; Chen, Y. *ACS Nano* **2008**, *2*, 463−470.

(13) Liu, H.; Zhang, L.; Guo, Y.; Cheng, C.; Yang, L.; Jiang, L.; Yu, G.; Hu, W.; Liu, Y.; Zhu, D. *J. Mater. Chem. C* **2013**, *1*, 3104.

(14) Pei, S.; Cheng, H.-M. *Carbon* **2012**, *50*, 3210−3228.

(15) Galpaya, D.; Wang, M.; Liu, M.; Motta, N.; Waclawik, E.; Yan, C. *Graphene* **2012**, *2012*, 30−49.

(16) Verdejo, R.; Bernal, M. M.; Romasanta, L. J.; Lopez-Manchado, M. A. *J. Mater. Chem.* **2011**, *21*, 3301.

(17) Ansari, S.; Kelarakis, A.; Estevez, L.; Giannelis, E. P. *Small* **2010**, *6*, 205−209.

(18) Wei, T.; Luo, G.; Fan, Z.; Zheng, C.; Yan, J.; Yao, C.; Li, W.; Zhang, C. *Carbon* **2009**, *47*, 2296−2299.

(19) Barroso-Bujans, F.; Fernandez-Alonso, F.; Pomposo, J. A.; Enciso, E.; Fierro, J. L. G.; Colmenero, J. *Carbon* **2012**, *50*, 5232−5241.

(20) An, X.; Simmons, T.; Shah, R.; Wolfe, C.; Lewis, K. M.; Washington, M.; Nayak, S. K.; Talapatra, S.; Kar, S. *Nano Lett.* **2010**, *10*, 4295−4301.

(21) Gudarzi, M. M.; Sharif, F. *Soft Matter* **2011**, *7*, 3432.

(22) Dao, T. D.; Erdenedelger, G.; Jeong, H. M. *Polymer* **2014**, *55*, 4709−4719.

(23) Zhang, L.; Shi, T.; Wu, S.; Zhou, H. *High Perform. Polym.* **2013**, *26*, 156−165.

(24) Yin, G.; Zheng, Z.; Wang, H.; Du, Q.; Zhang, H. *J. Colloid Interface Sci.* **2013**, *394*, 192−198.

(25) He, Y.; Wu, F.; Sun, X.; Li, R.; Guo, Y.; Li, C.; Zhang, L.; Xing, F.; Wang, W.; Gao, J. *ACS Appl. Mater. Interfaces* **2013**, *5*, 4843−4855.

(26) Dukhin, A. S.; Goetz, P. J. *Characterization of Liquids, Nano- and Microparticulates, and Porous Bodies using Ultrasound*; Elsevier: Oxford, UK, 2010.

(27) Woltornist, S. J.; Oyer, A. J.; Carrillo, J.-M. Y.; Dobrynin, A. V.; Adamson, D. H. *ACS Nano* **2013**, *7*, 7062−7066.

(28) Aveyard, R.; Binks, B. P.; Clint, J. H. *Adv. Colloid Interface Sci.* **2003**, *100−102*, 503−546.

(29) Wang, J.; Wolf, R. M.; Caldwell, J. W.; Kollman, P.; Case, D. *J. Comput. Chem.* **2004**, *25*, 1157−1174.

(30) Oyer, A. J.; Carrillo, J.-M. Y.; Hire, C. C.; Schniepp, H. C.; Asandei, A. D.; Dobrynin, A. V.; Adamson, D. H. *J. Am. Chem. Soc.* **2012**, *134*, 5018−5021.

(31) Frisch, M. J.; Trucks, G. W.; Schlegel, H. B.; Scuseria, G. E.; Robb, M. A.; Cheeseman, J. R.; Scalmani, G.; Barone, V.; Mennucci, B.; Petersson, G. A.; Nakatsuji, H.; Caricato, M.; Li, X.; Hratchian, H. P.; Izmaylov, A. F.; Bloino, J.; Zheng, G.; Sonnenb, J. Gaussian, 2009.

(32) Price, D. J.; Brooks, C. L. *J. Chem. Phys.* **2004**, *121*, 10096−10103.

(33) Kumar, S.; Rosenberg, J.; Bouzida, D.; Swendsen, R.; Kollman, P. *J. Comput. Chem.* **1995**, *16*, 1339−1350.

(34) Larson, R. *The Structure and Rheology of Complex Fluids*; Oxford University Press: New York, 1998.

(35) BASF. BASF Neopor http://www.neopor.basf.us/about/product-certification.

(36) Wang, S.; Zhang, Y.; Abidi, N.; Cabrales, L. *Langmuir* **2009**, *25*, 11078−11081.

(37) Coleman, J. N. *Adv. Funct. Mater.* **2009**, *19*, 3680−3695.

(38) Carreira, D. J.; Chu, K. **1986**, 797−804.

DOI: 10.1021/ma5024236
Macromolecules XXXX, XXX, XXX−XXX